Repeated logs in LL–03: dual–induction log (deep and medium penetration)
The repeated measurements with the dual–induction log (deep and medium penetration) show variations in resistivity even between different logs of one day, therefore these values cannot be used for an analysis of changes. More details can be found in the first annual PRENLAB-2 report.

Repeated logs in LL–03: sonic logs, P-wave travel times
The difference in the sonic velocity of logs measured at one day is in average 3.0% of the average value (Figure 19). At some depth intervals greater differences between repeated logs are caused by inaccurate depth matching, e.g. at 740 m in Figure 19. Depth intervals where the amplitude of the measured signal is very low showed significant variation in the (automatically) picked travel times, thus cannot be considered for an analysis of changes. Greater variations between logs of different logging campaigns could not be found.

Repeated logs in LL–03: neutron-neutron logs
Neutron-neutron logs were run before and after the June 2000 earthquakes. In the environment of borehole LL-03 at Nefsholt they are expected to reflect mainly the water content of the rock. They are plotted together in Figures 20 and 21. The one of April 1999 was measured with a log speed of 40 m/min. Those of October 1999 and August 2000, both were measured with a logging speed of 6 m/min. The April 1999 and the August 2000 logs were measured at 0.5 m depth interval. The 1999 log was measured at a depth interval of 0.1 m. The depth scale was shifted as described above.

Small changes can be found as well as between logs of April and October 1999 as between those of October 1999 and August 2000. The differences in logs of 1999 are larger than between those of October 1999 and August 2000. This might be due to the comparatively high logging speed in April 1999. At the depth of 465 m the neutron logs do not show a difference, as would be expected if a crack would have widened there. Generally, the match between the logs is remarkably good – so good that all of the observed differences can probably be attributed to statistical fluctuations.

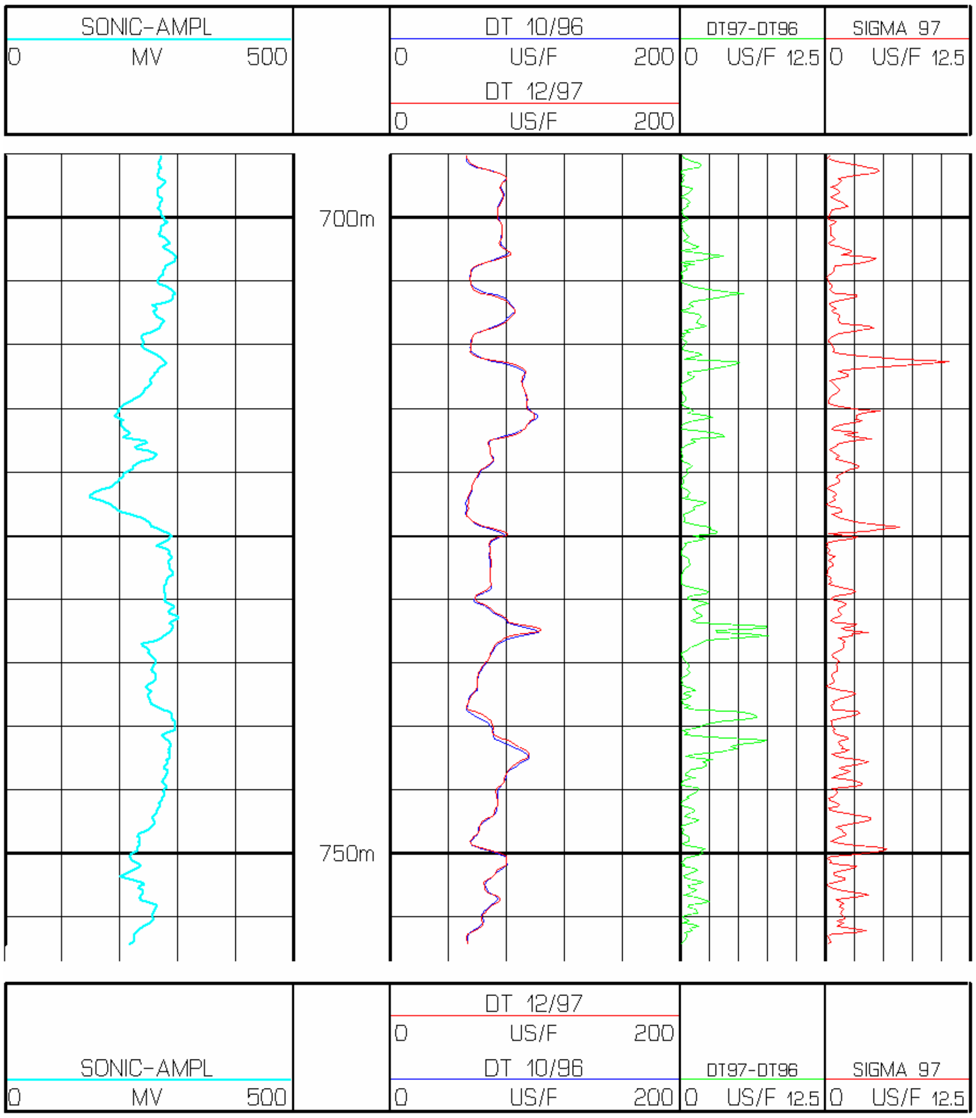

Figure 19. *Data example showing from left to right panel: an average curve of sonic amplitude, a superposition of the average compensated travel times measured in October 1996 and in December 1997 (each averaged over four runs performed immediately one after the other), the difference between these two average travel time curves (absolute value, green curve) and the standard deviation (absolute value) derived from the four runs performed in December 1997. Compensated travel times are given in microseconds per foot. The difference between the average travel times exceeds the standard deviation only in low amplitude intervals (not shown here) or at depths with inaccurate depth–matching (for example around 740 m).*

Borehole–televiewer measurements

Nefsholt:

In drillhole LL-03 (63.92°N, 20.41°W), the orientation of the borehole breakouts found is about 120.5° to 126°, implying a direction of the maximum horizontal principal stress of N30.5°E to N36°E. The circular standard deviation (1σ) is of the order of 10°. The stress direction is in agreement with the expected stress direction from large-scale tectonics (left–lateral strike-slip). The length of picked breakouts sums up to approximately 5.5 m. They are supposed to have formed while drilling, i.e. in 1977.

Þykkvibær:

Borehole breakouts have been found in the depth intervals 925 m to 927 m and 937 m to 941 m in THB-13 (63.77°N, 20.67°W). The breakouts in these two depth intervals sum up to approximately 3.5 m. Data quality is rather poor due to weak reflection amplitudes. Figure 22 shows a data example. The average breakout azimuth is between N105°E (upper depth–interval) and N121°E (lower depth–interval). Statistical analysis over the whole depth range gives a breakout–orientation of N111°E with a circular standard deviation (1σ) of about 10°. This would mean that the larger principal horizontal stress is in average oriented N21°E. This is in agreement with the stress directions expected from the overall tectonics as well as with the results from Nefsholt. The breakouts in THB-13 have most likely formed during drilling in 1997, i.e. just before they were measured.

Böðmóðsstaðir

No breakouts have been observed in borehole BS-11 (64.20°N, 20.55°W), but there are vertical fractures visible between 713 m and 934 m depth. The length of the vertical fractures sums up to 45 m. Vertical fractures are expected to occur in the direction of the maximum horizontal principal stress because of tensile failure of the borehole wall. They are supposed to be not of natural origin but drilling induced; so they stem out of 1992. These fractures occur at an azimuth of N45°E to N90°E. A data example is presented in Figure 23.

Breakout orientations and fracture statistics from the measurements in the SISZ are shown in Table 5 and Figure 24 as an overview. In Subpart 7B stress orientations were calculated for the SISZ using the co-seismic stress release of large earthquakes in the SISZ since 1706 and taking into account the stress build-up by plate motion. For comparison, we give the values for the boreholes where measurements were performed in Figure 25. Both results show stress orientations similar to each other. In general, the modelled values are more oriented to E-W than the measured ones.

Well:	Logged interval:	Interval with BOs / vert. fractures:	Total length of BOs/ vert. fractures:	Orientation of σ_H:	circ. std. devi.:
BS-11	703-1090 m	713-934 m	45.0 m fract.	N45°E–N90°E	—
LL-03	80-1100 m	780-983 m	5.0 m BOs	N30°E	12°
THB-13	466-1225 m	925-941 m	3.5 m BOs	N21°E	10°

Table 5. *Stress orientations found from borehole–televiewer logs.*

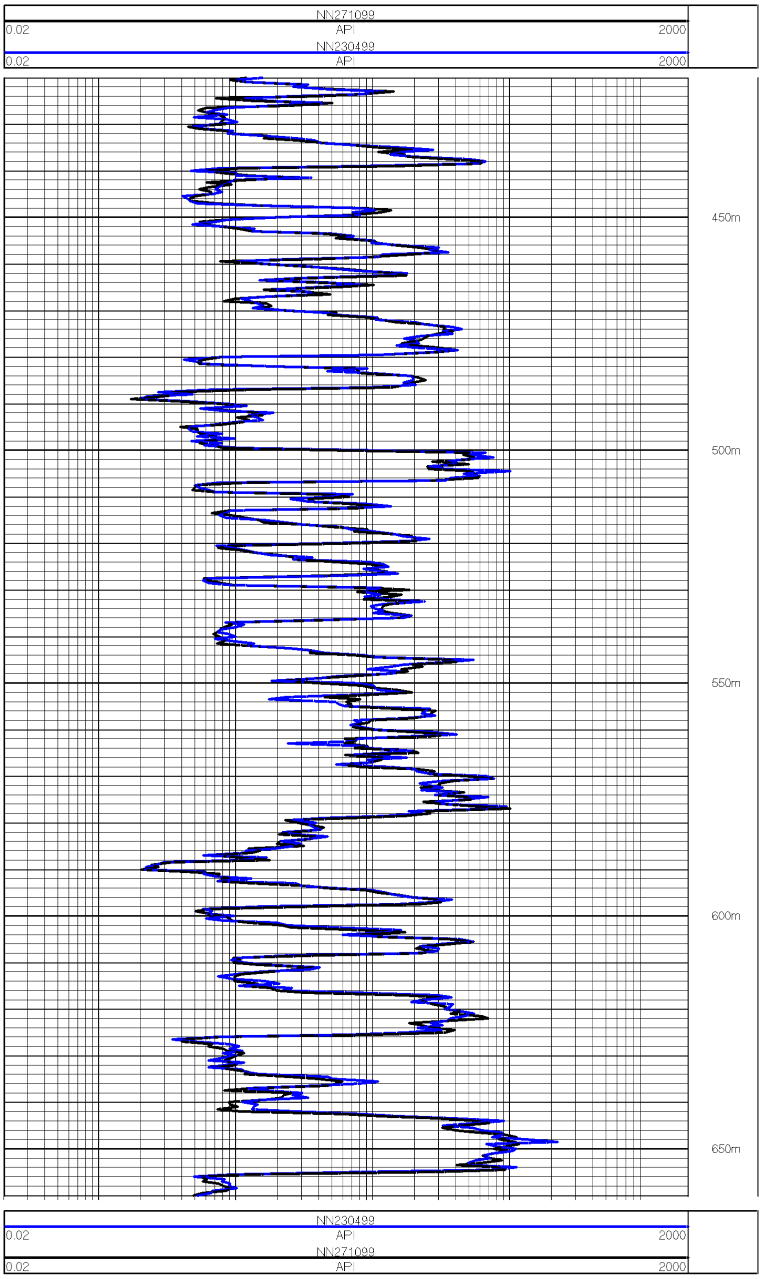

Figure 20. *Data example comparing short (SN) and long normal (LN) resistivity data from April 1999 and October 1999.*

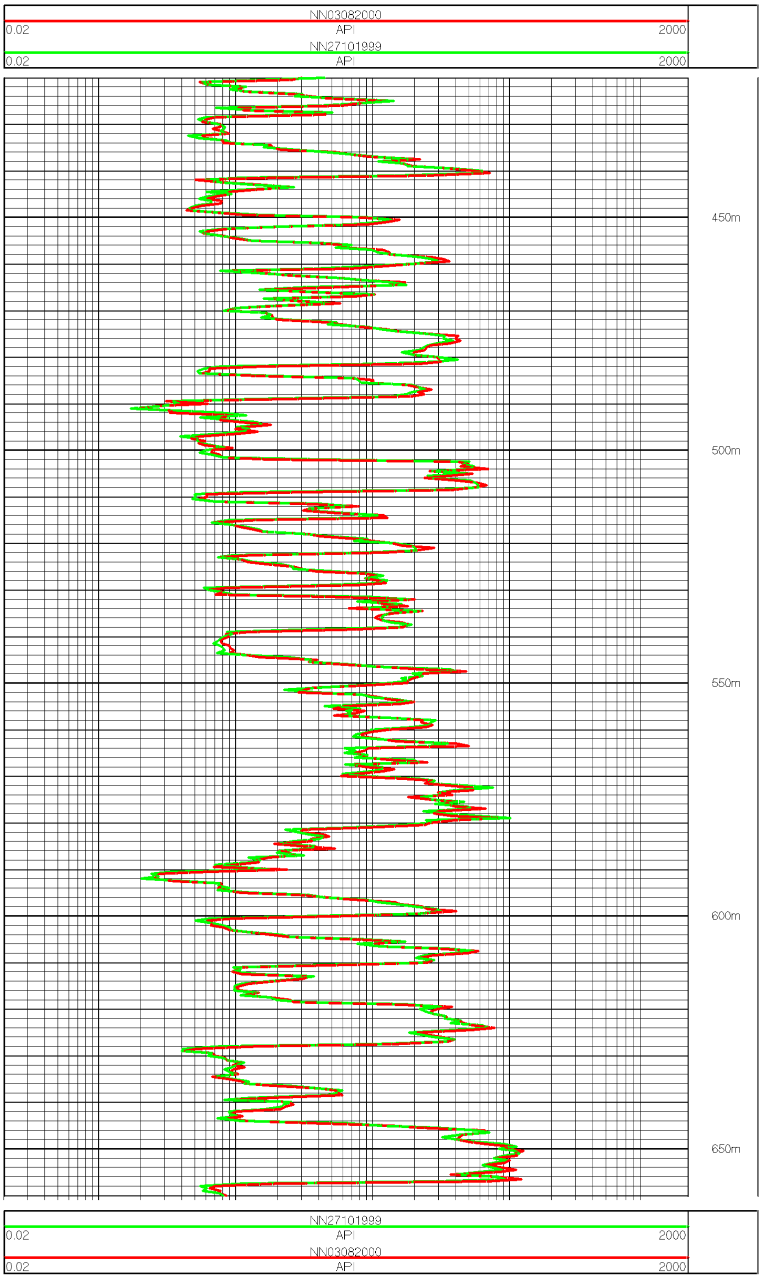

Figure 21. *Data example comparing short (SN) and long normal (LN) resistivity data from October 1999 and August 2000.*

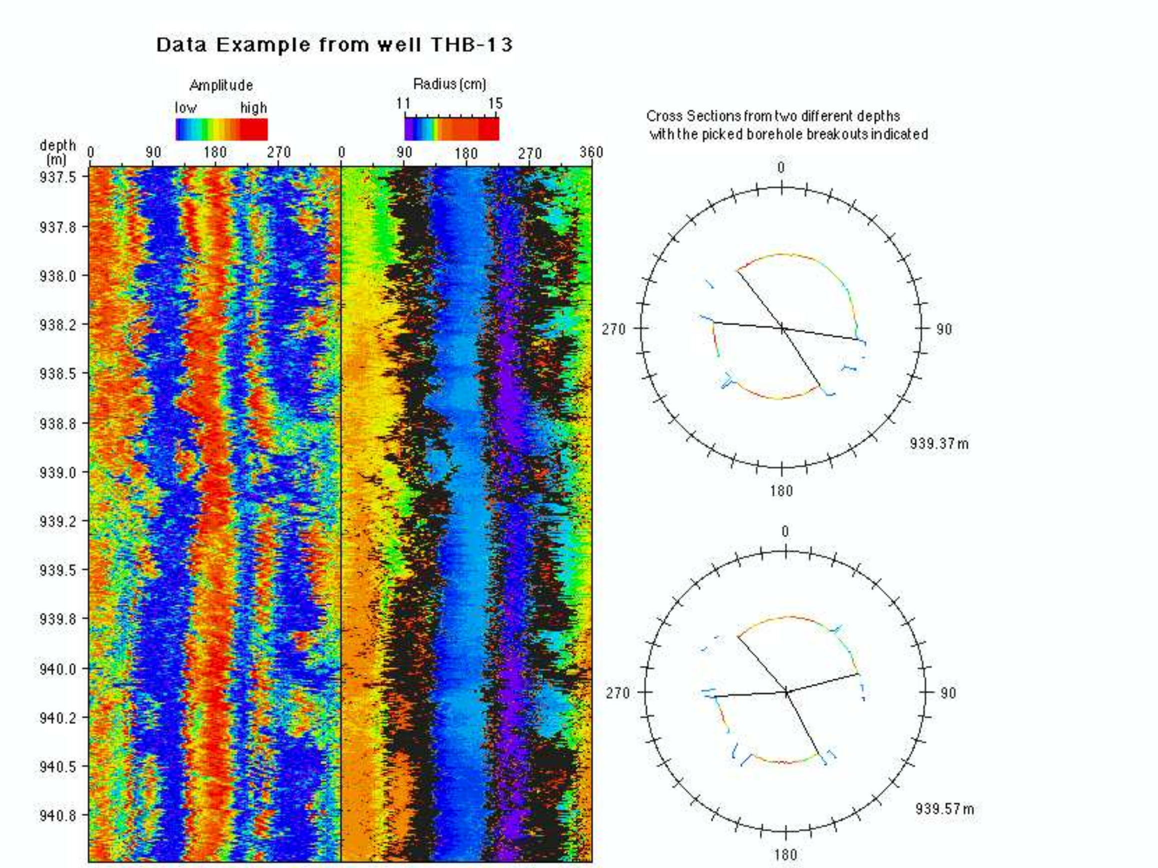

Figure 22. *Example of the borehole breakouts found in well THB-13 with two cross sections. The two panels show the amplitude of the reflected signal (left) and the radius calculated from the travel time (right), both unwrapped from north over east, south, west to north. Vertical axis: depth in meters. Breakouts appear as vertical bands of low reflection amplitudes. Due to poor reflection amplitudes, the values for the radius are often missing in these parts, resulting in black bands. In the two cross sections, the black lines indicate the range in azimuth of the picked breakouts.*

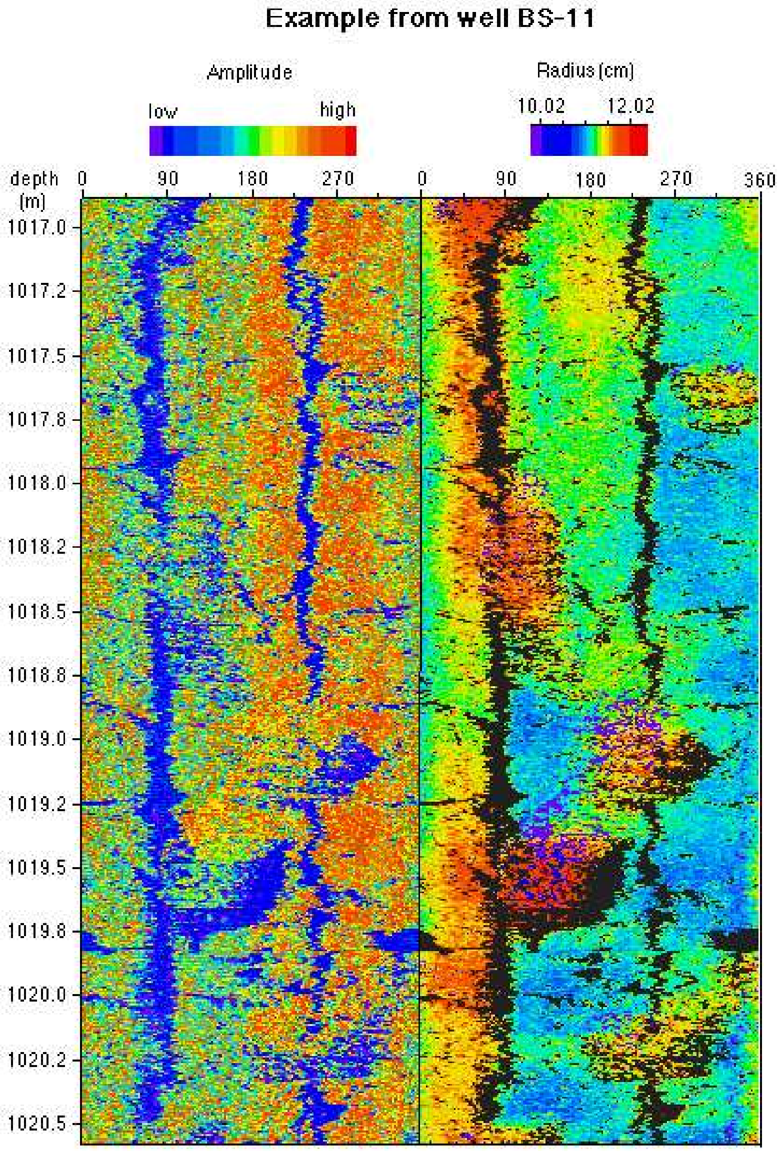

Figure 23. *Example for drilling induced vertical fractures observed in borehole BS-11. The data are displayed as described in Figure 22. The fractures appear as narrow vertical stripes of low reflection amplitude, much narrower than breakouts. Values for the radius calculated from travel time are missing for these stripes due to low amplitudes.*

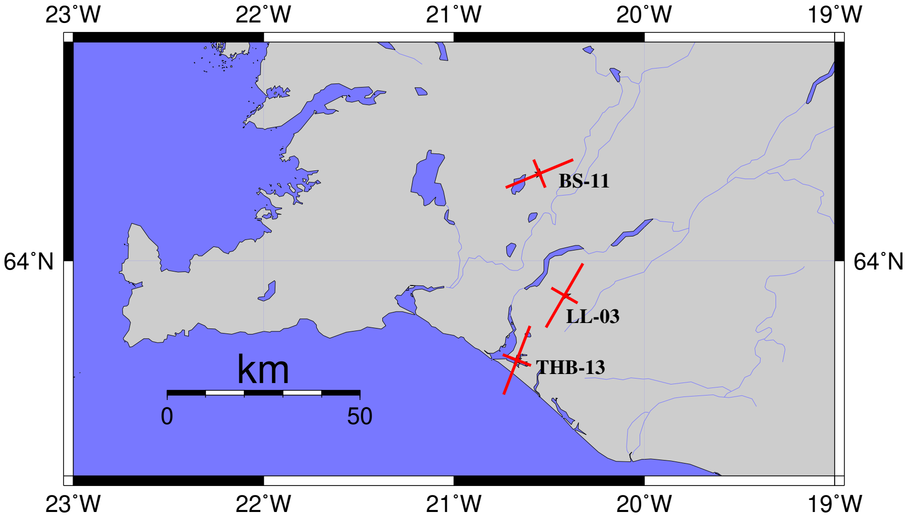

Figure 24. *Stress orientations found in boreholes in the South Iceland seismic zone. Long red lines indicate the orientation of the larger, short ones that of the lower principle horizontal stress.*

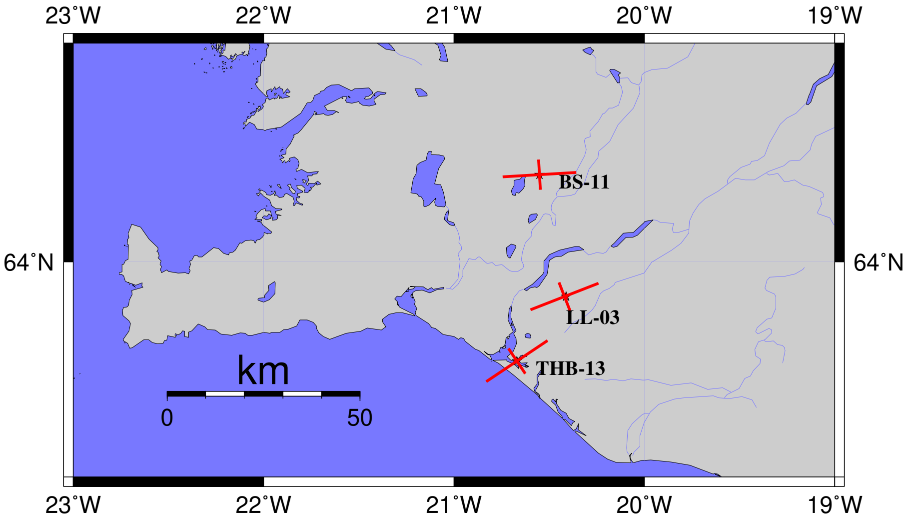

Figure 25. *Stress orientations calculated in Subpart 7B for borehole positions in and near the SISZ.*

Summary:
The results can be summarized as follows:

- The measurements at LL-03 for changes in P–wave velocity with the sonic log, for porosity changes with the neutron-neutron log, and for resistivities with the latero log, 16", and 64" show good repeatability.

- The earthquakes in June 2000 happened two weeks before the end of PRENLAB-2 project. Therefore, the last logging campaign before the events took place 8 months before the events. No clear indication for changes before the events was found. This might be, because the time difference was too long or the signals were below the detection threshold of the tools used.

- Coseismic changes might be visible at about 465 m depth, where both the 16" and the 64" log show a decrease in resistivity. It would be interesting to check whether cracks can be found there and at the other feed-points (visible in the temperature logs) with a high resolution borehole televiewer.

- Non-vertical fractures found down to nearly 1100 m depth show the same dominant strike as those observed at the surface (see first annual PRENLAB-2 report). A dependence of fracture orientation upon depth or upon geographical latitude could not be found.

- The stress orientations found at all three locations are similar and agree with a left–lateral strike-slip regime. They are based on data that are assumed to originate from 1977, 1992 and 1997 and are not perpendicular to existing ruptures found in the SISZ and, therefore indicate, that the SISZ is not a weak fault, as postulated for the San Andreas fault. Instead, it appeared prepared for another earthquake. From a rock mechanics view the stress directions found at LL-03 and THB-13 correlate with N-S striking faults, as they are found in the SISZ. On the other hand the orientation of maximum horizontal principal stress found at BS-11 correlates with the model of an E-W striking strike-slip fault zone. A linear dependency of stress orientation on age, depth or geographical position (in-/outside the SISZ) of the boreholes could not be found. Stress orientations similar to ours were also found by Stefánsson et al. (1993) from fault plane solutions. This was confirmed by other groups in the framework of PRENLAB as by Bergerat and coworkers (Subproject 6), who found a mean orientation of σ_H of N56°E derived from 1916 fault plane solutions selected from 48669 earthquakes in the SISZ of the years 1995 to 1997 (Angelier et al. 2000). A NE–SW orientation of σ_H was also the result of investigations of Crampin and coworkers on shear-wave splitting due to stress anisotropy at four of six seismic stations in the SISZ (Crampin et al. 1999) (Subproject 3).

Participants:
Besides the proposer and the subcontractor, the following scientists and technicians have supported the Subproject:
G. Axelsson (OS), H. Bäßler (Karlsruhe), C. Carnein (GFZ), E.T. Elíasson (OS), H.-J. Fischer (GFZ), P. Fleckenstein (GFZ) S.Þ. Guðlaugsson (OS), K. Henneberg (GFZ; now at

PGS, Oslo), G. Hermannsson (OS), M. Hönig (GFZ), G. Kurz (GFZ; now at NLfB–GGA, Hannover), Fernando J. Lorén Blasco (GFZ), S. Mielitz (GFZ), H. Sigvaldason (OS), Ó. Sigurðsson (OS), and B. Steingrímsson (OS).

3.4.4 Acknowledgements

We are very grateful to all above named participants. We thank Orkustofnun for excellent preparation and support of the logging campaigns. We like to thank the owners of the boreholes for their permission to work in the wells. We are very grateful to GeoSys company and the Geophysical Institute of Karlsruhe University for lending us a BHTV and additional equipment for the logging campaign in June 1998. We also thank the GFZ logging team very much. We are also indebted to F. Lorenzo Martín for assisting in the graphics and checking the text.

3.4.5 References

Angelier, J., F. Bergerat & C. Homberg 2000. Variable coupling explains complex tectonic regimes near oceanic transform fault: Flateyjarskagi, Iceland. *Terra Nova*, in press.

Crampin, S., T. Volti & R. Stefánsson 1999. A successfully stress-forecast earthquake. *Geophys. J. Int.* 138, F1-F5.

Stefánsson, R., R. Böðvarsson, R. Slunga, P. Einarsson, S.S. Jakobsdóttir, H. Bungum, S. Gregersen, J. Havskov, J. Hjelme & H. Korhonen 1993. Earthquake prediction research in the South Iceland seismic zone and the SIL project. *Bull. Seism. Soc. Am.* 83, 696-716.

Zoback, M.D., M.L. Zoback, V.S. Mount, J. Suppe, J. Eaton, J.H. Healy, D. Oppenheimer, P. Reasenberg, L. Jones, C.B. Raleigh, I.G. Wong, O. Scotti & C. Wentworth 1987. New evidence on the state of stress on the San Andreas fault system. *Science* 238, 1105-1111.

3.5 Subproject 5: Active deformation determined from GPS and SAR

Contractor:

Freysteinn Sigmundsson
Nordic Volcanological Institute
Grensásvegur 50
108 Reykjavík
Iceland
Tel: +354–525–4494
Fax: +354–562–9767
E–mail: fs@norvol.hi.is

Associated contractor:

Kurt L. Feigl
Centre National de la Recherche Scientifique
UPR 0234 - Dynamique Terrestre et Planétaire
14 Avenue Edouard Belin
FR–31400 Toulouse
France
Tel: +33–5–6133–2940
Fax: +33–5–6125–3205
E–mail: kurt.feigl@cnes.fr

Subcontractor:

Páll Einarsson
Science Institute
University of Iceland
Hofsvallagata 53
107 Reykjavík
Iceland
Tel: +354–525–4816
Fax: +354–552–8801
E–mail: palli@raunvis.hi.is

Researcher:

Sverrir Guðmundsson
Nordic Volcanological Institute
Grensásvegur 50
108 Reykjavík
Iceland
Tel: +354–525–5868
Fax: +354–562–9767
E–mail: sg@raunvis.norvol.hi.is

Researcher:
Amy E. Clifton
Nordic Volcanological Institute
Grensásvegur 50
108 Reykjavík
Iceland
Tel: +354–525–5481
Fax: +354–562–9767
E–mail: amy@norvol.hi.is

The main end results of this Subproject are described in the following. For details of how individual tasks were carried out, we refer to PRENLAB-2 first annual report.

3.5.1 Subpart 5A: SAR interferometry study of the South Iceland seismic zone

The objective was to measure ongoing crustal deformation in the South Iceland seismic zone (SISZ) and relate it to distribution of faults and seismicity there. We have met that objective at the western edge of the SISZ, around the Hengill volcanic center, and published the results in an international, peer-reviewed scientific journal (Feigl et al. 2000).

We have analyzed synthetic aperture radar (SAR) images acquired by the ERS-1 and ERS-2 satellites between July 1993 and September 1998 using interferometry. In spite of our careful image selection, correlation is poor in the relatively flat and wet lowlands of southern Iceland, which unfortunately includes most of the faults in the SISZ. On the other hand, coherence remains good, even after 4 or 5 years, in the mountainous areas around Hengill.

The predominant signature in all the interferograms spanning at least 1 year, is a concentric fringe pattern centered just south of the Hrómundartindur volcanic center (Figure 26). This we interpret as mostly vertical uplift caused by increasing pressure in an underlying magma source. The volume source that best fits the observed interferograms lies at 7±1 km depth and remains in the same horizontal position to within 2 km. It produces 19±2 mm/year of uplift. This deformation accumulates as elastic strain energy at a rate 2.8 times the rate of seismic moment release.

Under our interpretation, magma is injected at 7 km depth, just below the seismogenic zone formed by colder, brittle rock. There, the inflation induces stresses that exceed the Coulomb failure criterion, triggering earthquakes. Accumulated over 5 years, the deformation increases the Coulomb failure stress by >0.6 bar in an area that includes some 84% of the earthquakes recorded between 1993 and 1998 (Figure 27 and Figure 28).

Our model suggests that magmatic inflation can trigger earthquakes, with stress rising slowly to failure and then dropping instantaneously in an earthquake. Thus a plot of stress as a function of time on a given fault forms a sawtooth pattern. Prior to an earthquake, on the leading edge of the sawtooth, the stress increases at a rate of the order of $\sim$ 1 bar/year. After accumulating for a time interval Δt years, the stress then decreases abruptly in an earthquake with stress drop $\delta\tau$. For the magnitude 5.2 earthquake of June 4, 1998, we take a mean stress drop of the order of $\tau \sim 20$ bars, assuming that μ =33 GPa and $\delta\tau = \mu U(LW)^{1/2}$. If this rupture returns the state of its stress to its initial level, then the accumulation interval is of the order of $\Delta t \sim 20$ years. If this process is cyclical, then this interval is the recurrence time of a characteristic earthquake. It suggests that inflation of a magma chamber can furnish the primary driving force to actually break rocks on a fault in an earthquake.

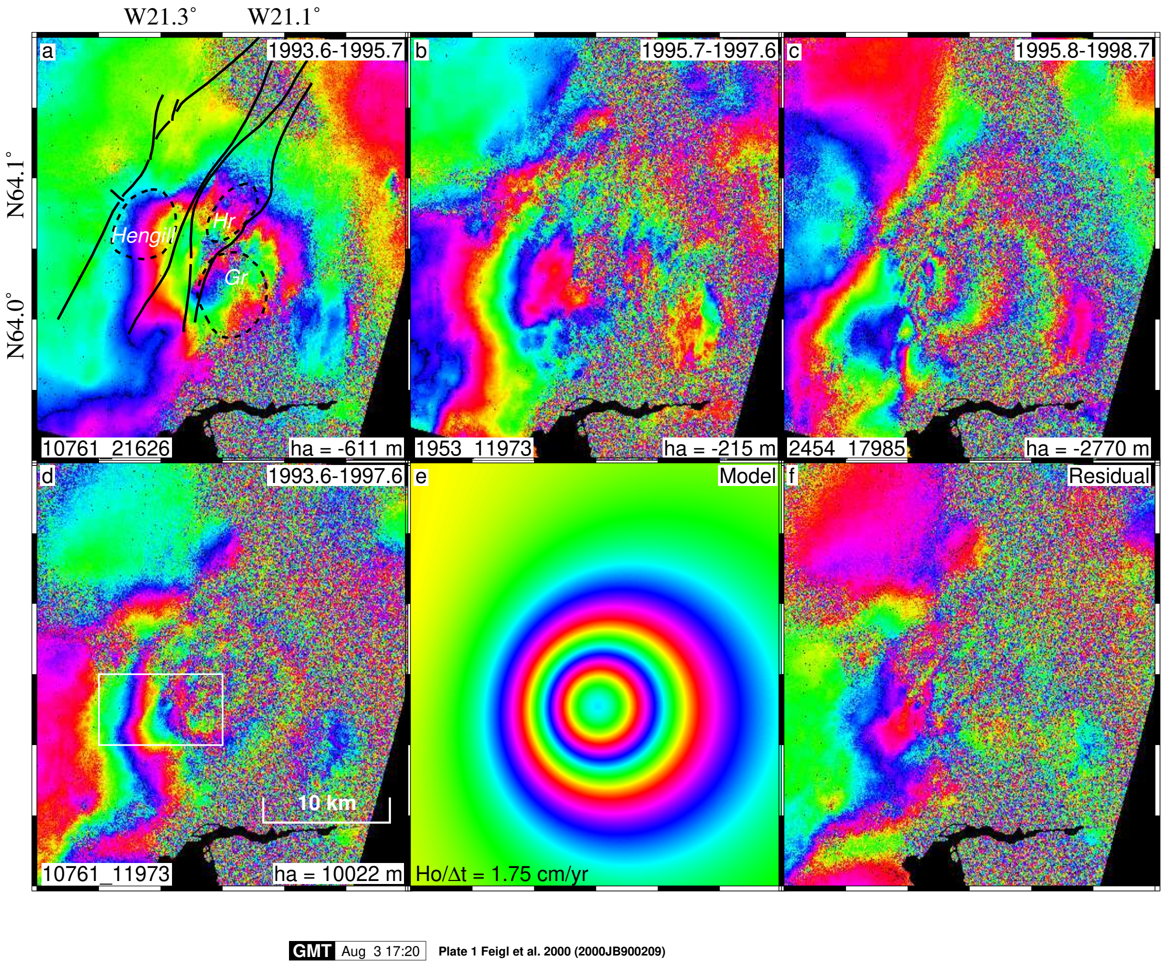

Figure 26. *Observed interferograms of the Hengill area for four different time intervals. The time interval appears in the upper right corner of each panel, the orbit numbers appear at lower left, and the altitude of ambiguity h_a appears at lower right. One fringe represents 28 mm of range change. Two concentric fringes are visible in the 4-year interferogram (d) indicating at least 6 cm of uplift between August 1993 and August 1997. The white box in (d) includes the discontinuity enlarged in (b) and (c).*

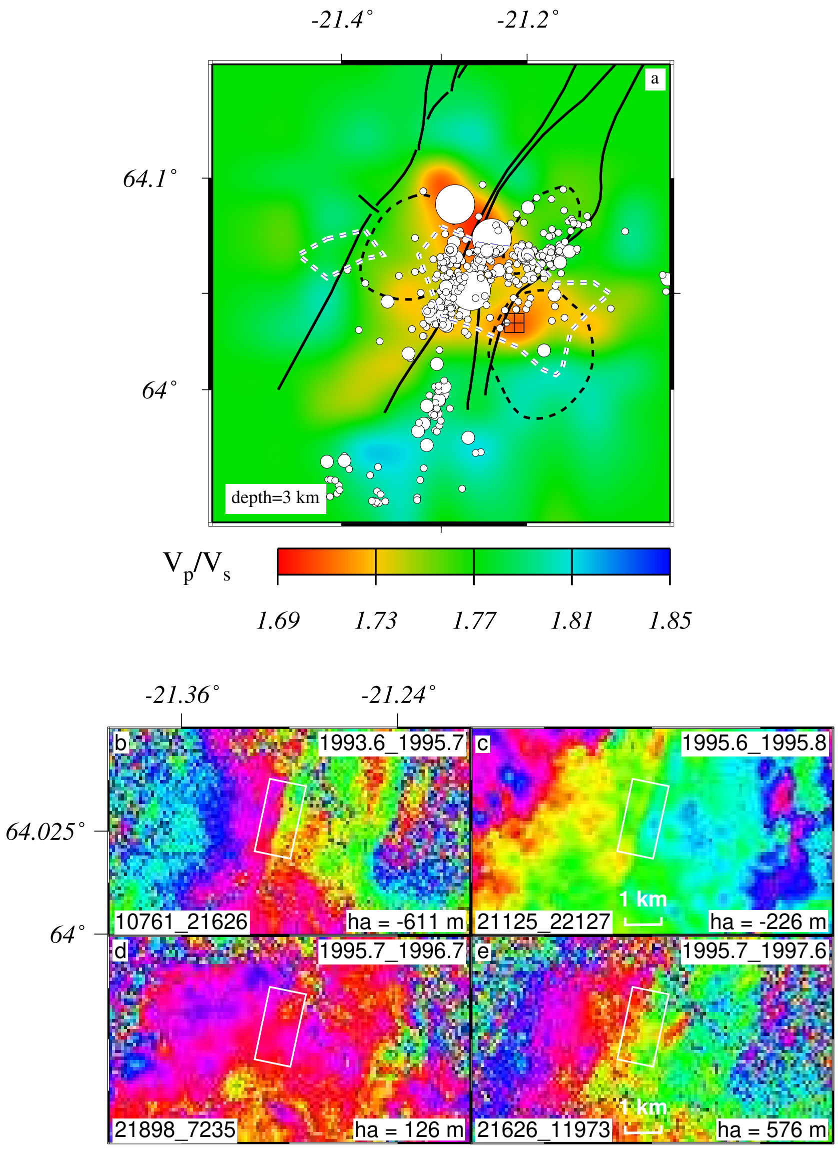

Figure 27. *(a) Structural map showing V_P/V_S wave speed ratio at 4 km depth (Miller et al. 1998); our best fitting volume source (crossed square); contours of P-wave speed velocity anomaly $\delta V_P = +1\%$ at 4 km depth (dashed white lines); contours of Miller et al. (1998); limits of volcanic system (solid black lines); outlines of three central volcanos (dashed black lines). Circles and dots show earthquake hypocenters for events between 1993 and 1998 (Rögnvaldsson et al. 1998a; Rögnvaldsson et al. 1998b). The largest circle is the M_w=5.2 event of June 4, 1998. Events with magnitude smaller than 2.5 plot as dots. (b-e) Enlargement of two interferograms that span August 1995 [b) and c)], and two which do not [d) and e)]. A discontinuity is clearly visible in b) and c) and is interpreted as a fault rupturing. We cannot discern a discontinuity in Figures d) and e).*

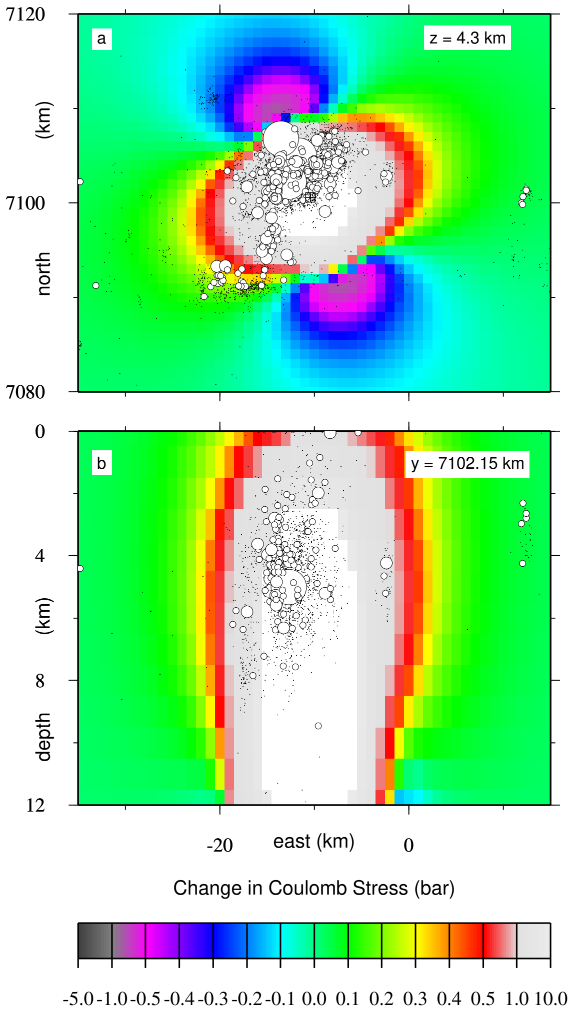

Figure 28. *(a) Coulomb failure stress change on optimally oriented vertical faults shown in a horizontal slice at 4.3 km depth. White color denotes where the stress increase is >1 bar but <10 bar. Source parameters include: latitude* 64.032°*N, longitude* 21.213°*W, depth 7.0 km, tensile opening 12.1 m on each of three dykes with length L=1 km and width W=1 km; the apparent coefficient of friction* $\mu'_f=0.4$*, the azimuth* $\phi=70°$ *(measured clockwise from north) of the most compressive principal value of the stress tensor, and its magnitude* $|\sigma_1|=1$ *bar, and the two Lame' constants* $\mu=\lambda=33$ *GPa. Hypocenters of the earthquakes (circles and dots) are as in Figure 27. (b) Coulomb failure stress change on optimally oriented vertical faults shown in a vertical cross section passing E-W through the center of the modelled volcanic point source (crossed square). Model parameters and plotting conventions as in Figure 27a.*

3.5.2 Subpart 5B: GPS measurements of absolute displacements

The objective was to measure absolute plate motions near the South Iceland seismic zone (SISZ), in order to help with improved understanding of the mechanism of faulting in the seismic zone. The objective has been met by developing a new technique to combine GPS and satellite radar interferograms into three-dimensional motion maps, that give an unprecedented view of the absolute plate motions (Guðmundsson et al. 2000). The methodology has been applied to the western continuation of the SISZ, the Reykjanes peninsula.

The original plan was to operate one semi-continuous GPS station and interpret data from this station. Rather than doing that, we participated in the installation of network of continuously recording stations in S-Iceland. These results are described in Subproject 1. Additional work was conducted on two topics: Development of a new technique to combine GPS and satellite radar interferometry results (work lead by Sverrir Guðmundsson), and secondly, fault mapping was conducted in the Hengill region in order to advance further the understanding of interferograms collected in Subpart 5A (work lead by Amy Clifton).

The new technique developed to efficiently produce high-resolution three-dimensional surface motion maps, relies on combining information about motion of the earth's surface from interferometric observations of synthetic aperture radar images and repeated Global Positioning System geodetic measurements. Unwrapped interferograms showing pixel-wise change in range from ground to satellite, and sparse values of three-dimensional movements are required as input. The problem of finding the full three-dimensional motion field is separated into two two-dimensional problems. Initially the vertical component of the deformation field, and its horizontal component in the look-direction of the satellite are found. Later the look-direction component is resolved into north and east components. Initial values for the motion fields are assigned to each pixel of interferograms from ordinary kriging of available GPS observations. These values are then updated and optimized by comparison with the interferograms and the GPS observations. Additional constraint is the smoothness of motion field. Markov random field based regularization, and simulated annealing algorithm are used for the optimization. The technique has been applied to create surface motion maps for the Reykjanes peninsula (Figure 29). Although separate interpretation of GPS and InSAR data from the area (Hreinsdóttir et al. 2000; Vadon and Sigmundsson 1997) have shown the main components of deformation, the three-dimensional motion maps provide an unprecedented view of the three-dimensional deformation. The largest signals are plate movements causing large gradients in the east motion field, and circular subsidence centered on the Svartsengi and Eldvörp geothermal area. The north and east motion field images show also clearly that the subsidence is associated with horizontal movements towards the subsidence center, a pattern that is imprinted on the background plate movements. The motion maps form the basis of a future project on conducting a detailed study of strain accumulation in the area and how it correlates with seismicity.

A related effort was the study of faulting and surface rupture that has taken place in the Hengill volcanic area (Clifton and Sigmundsson 2000). It is the same area as studied by satellite radar interferometry under Subpart 5A. The Hengill and Hrómundartindur volcanic systems in SW-Iceland are considered to comprise the Hengill triple junction at which the oblique Reykjanes peninsula rift zone, the western volcanic (rift) zone and the South Iceland seismic (transform) zone meet. It is therefore experiencing both tectonic extension and left-